Location of the heme-Fe atoms within the profile structure of a monolayer of cytochrome *c* bound to the surface of an ultrathin lipid multilayer film

James M. Pachence, Robert F. Fischetti, and J. Kent Blasie
Chemistry Department, University of Pennsylvania, Philadelphia, Pennsylvania 19104

ABSTRACT We have recently developed x-ray diffraction methods to derive the profile structure of ultrathin lipid multilayer films having one to five bilayers (e.g., Skita, V., W. Richardson, M. Filipkowski, A.F. Garito, and J.K. Blasie. 1987. *J. Physique.* 47:1849–1855). Furthermore, we have employed these techniques to determine the location of a monolayer of cytochrome *c* bound to the carboxyl group surface of various ultrathin lipid multilayer substrates via nonresonance x-ray diffraction (Pachence, J.M., and J.K. Blasie. 1987. *Biophys. J.* 52:735–747). Here an intense tunable source of x-rays (beam line X9-A at the National Synchrotron Light Source at the Brookhaven National Laboratory) was utilized to measure the resonance x-ray diffraction effect from the heme-Fe atoms within the cytochrome *c* molecular monolayer located on the carboxyl surface of a five monolayer arachidic acid film. Lamellar x-ray diffraction was recorded for energies above, below, and at the Fe *K*-absorption edge ($E = 7,112$ eV). An analysis of the resonance x-ray diffraction effect is presented, whereby the location of the heme-Fe atoms within the electron density profile of the cytochrome *c*/arachidic acid ultrathin multilayer film is indicated to ± 3 Å accuracy.

INTRODUCTION

Structural techniques such as nonresonance and resonance x-ray diffraction and neutron diffraction have succeeded in providing reasonably detailed structural information concerning the overall structural organization of membranes as well as the structures of their molecular components (1–6); these previous studies employed thick, oriented multilayer systems (1–6). It was recently found these same techniques can be utilized to derive significant structural information for ultrathin lipid multilayer films containing 1 to 20 bilayers, which provided some important advantages over using the thick, oriented multilayer systems (7–10). For example, nonresonance x-ray diffraction techniques were used to derive the electron density profile structures of periodic and nonperiodic ultrathin multilayer films prepared via the Langmuir-Blodgett technique (7–10); these initial studies showed that the electron density profile of each individual monolayer within either a periodic or nonperiodic multilayer lattice can be calculated to a resolution of < 5 Å. As a result, small differences in the configuration an/or composition of an individual monolayer within the multilayer profile structure could be determined (10). Furthermore, the development of these techniques has led to the determination of the location of a monolayer of cytochrome *c* bound to the carboxyl group surface of various ultrathin multilayer substrates via nonresonance x-ray diffraction (7).

Resonance x-ray diffraction has been shown to be a powerful tool to determine with high precision the position of selected atoms within the structure of noncrystalline systems of biomolecular complexes, including thick, oriented membrane multilayers (11–14). For example, this technique was used to directly determine the position of the iron atom magnetically coupled with the primary quinone electron acceptor of a bacterial photosynthetic reaction center as well as the heme iron atom of the cytochrome *c* electron donor that is electrostatically bound to this integral membrane protein, within the profile structure of reconstituted membranes, containing a reaction center-cytochrome *c* complex (13).

Here we describe the utilization of resonance x-ray diffraction (employing synchrotron radiation) to determine directly the location of the heme iron atom within the profile structure of a cytochrome *c* monolayer electrostatically bound to the surface of an ultrathin lipid film (five monolayers of arachidic acid). First, we establish that the resonance x-ray diffraction effect can be observed from the heme iron atoms located in the single monolayer of cytochrome *c*; we then show that the measured resonance x-ray diffraction effect can accurately position these iron atoms within the profile structure of such ultrathin lipid film/protein complexes.

MATERIALS AND METHODS

Materials

Arachidic acid and octadecyltrichlorosilane were purchased from Aldrich Chemical Co., Inc., Milwaukee, WI. Arachidic acid was zone

0006-3495/89/08/329/11 $2.00

refined with 50 passes at a rate of 1 cm/h and the purity of the center fraction was confirmed by differential scanning calorimetry (model 990; DuPont Co., Wilmington, DE). Type I cytochrome *c* was obtained from Sigma Chemical Co. (St. Louis, MO).

Methods

The preparation of the multilayers via the Langmuir-Blodgett technique was previously described (7–10) and will only be summarized. Flat glass plates (11 × 25 × 1 mm^3) were coated with octadecyltrichlorosilane (OTS), according to the method of J. Sagiv (15) to form a hydrophobic substrate. A monomolecular layer of arachidic acid was spread on a clean air-water interface. A subphase of 1 mM solution of $CdCl_2$ in filtered water (Millipore Corp., Bedford, MA), pH = 5.5 ± 0.2, temperature 17.5°C, was used in a Lauda Langmuir trough system (Beckman Instruments, Westbury, NY). The lipid monolayers were compressed to a constant surface pressure of 20 dyn/cm that was maintained during deposition. The substrates were passed through the lipid monolayer-water interface cyclically at a rate of 3 mm/min thereby depositing one monolayer film per pass. A 10 ml glass vial was placed in the subphase directly below the dipping mechanism before forming the lipid monolayer on the subphase. An odd number of monolayers (five in this instance) were deposited onto the substrate (providing a hydrophilic outer surface of carboxyl groups), and the glass slide was dropped directly into the glass vial. In this manner, the hydrophilic multilayer film surface was always in contact with the polar solvent. The glass vial was then placed into a 500 ml container of buffer (1 mM $NaHCO_3$ at pH 8) and allowed to equilibrate for 24 h. The cadmium-free buffer was changed twice over the next 24 h period.

The five monolayer arachidic acid films were then incubated for 48 h or more in 10 μM cytochrome *c* solution in 1 mM $NaHCO_3$, pH 8. The ultrathin multilayer film was removed from the cytochrome *c* solution, and incubated with 1 mM $NaHCO_3$ for 2 h or more. The buffer was changed every 5 min until there was no detectable cytochrome *c*, measured spectrophotometrically in the supernatant.

Data collection

Meridional x-ray diffraction data from the multilayer thin films were recorded as a function of the vector $\mathbf{q}_z$ ($\mathbf{q}_z = (2 \sin \theta)/\lambda$) corresponding to elastic photon momentum transfers parallel to the *z*-axis defined as normal to the substrate plane. Diffraction maxima along $\mathbf{q}_z$ arise from the two-dimensional projection of the electron density within the multilayer planes at constant value of *z* onto the *z*-axis. This projected electron density distribution is referred to as the electron density profile for the multilayer $\rho_{ml}(z)$.

The x-ray diffraction data for the cytochrome *c*/5-monolayer arachidic acid multilayer films were collected using the Biostructures Participating Research Team's beam line X-9A at the National Synchrotron Light Source at Brookhaven National Laboratory. The synchrotron has a bending magnet radius of 6.834 m, and was run at an electron energy of 2.5 GeV with a current range of 65 to 190 mA (average ≈ 90 mA). The x-ray wavelength (λ) was selected using a double Si crystal (111, nondispersive mode) monochromator which was 1,198 cm from the source, producing a line collimated x-ray beam that is intercepted by cylindrically bent horizontal mirror (Ni-coated aluminum, 50 × 80 cm) with its center at 1,340 cm from the source. The multilayers were placed on the ω-axis of a Huber 4-circle diffractometer, with the x-ray beam line-focused parallel to the ω-axis (substrate plane) and intercepting the substrate at grazing angles of incidence, ω. The mirror was bent to produce a vertically focused line of 0.15 mm (FWHM) at 50–60 cm from the diffractometer center (that was 1,580 cm from the source). A low impedance linear position sensitive detector (PSD) was positioned on the 2θ axis with its active length aligned in the 2θ plane along $\mathbf{q}_z$; the specimen to detector distance was 34 cm (He path). The full 100 mm active length of the PSD was digitized into 1,024 channels by a multichannel analyzer. Diffraction patterns from similar samples recorded on two-dimensional position-sensitive detectors have shown that no arcing is associated with the observable diffraction maxima along $\mathbf{q}_z$, because the multilayers have mosaic spreads of <0.01° (8–10); hence, the full height of the diffracted line-focused beam was intercepted by the 3mm high entrance aperature of the PSD for all diffraction maxima. For the present setup, the x-ray optics and the PSD spatial resolution result in a $\Delta\mathbf{q}_z$-resolution of < 0.001 $Å^{-1}$.

Oscillation diffraction patterns $I_e(\mathbf{q}_z)$ were recorded by rotating the multilayers over the angular range $0.1° < \omega < 5.0°$ with $\Delta\omega = 0.01°$ during data collection; 32 oscillations within this range were done for each energy value, which required ~10 min. The oscillation scans were under automated control by a PDP 11/24 computer (Digital Equipment Corp., Marlboro, MA). The multilayers were all maintained at a relative humidity of 98% (using a saturated salt solution of K_2SO_4), and the samples were at room temperature during the experiment.

The meridional diffracted intensity functions $I_e(\mathbf{q}_z)$ were corrected for meridional background scattering by subtracting a piecewise continuous two-exponential function as described previously (7). The intense "specular scattering" from the substrate (total external reflection of x-rays) dominates the diffraction at very small values of $\mathbf{q}_z < 0.007$ $Å^{-1}$, and is the major contribution to the background scattering. The intensity function $I_e(\mathbf{q}_z)$ was further corrected by a Lorentz factor $\mathbf{q}_z$ to compensate for the oscillation of the multilayers about ω. The background scattering and Lorentz corrected meridional intensity function $I_c(\mathbf{q}_z)$ was then taken to be proportional to the structure factor modulus squared $|F_{ml}(\mathbf{q}_z)|^2$ for the multilayer electron density profile $\rho_{ml}(z)$.

Data analysis: resonance x-ray scattering

The scattering factor for the *j*th resonant atoms in the structure of interest which possess an absorption edge for x-rays at the energy E_{edge} (due primarily to excitation of *K*-shell or *L*-shell electrons into the continuum) can be expressed as:

$$f_j(\mathbf{q}_z, E) = f_j^\circ(\mathbf{q}_z) + f_j'(\mathbf{q}_z, E) + \mathrm{i}f_j''(\mathbf{q}_z, E), \quad (1)$$

where f° is the nonresonance atomic scattering factor far away (>100 eV) from the absorption edge, f' is the resonance change in the real component of the atomic scattering factor (energy dependent), and f'' is the resonance change in the imaginary component (energy dependent); see reference 14. For Fe, the f' component is nonzero in particular for $E_{edge} - 50$ eV $< E < E_{edge} + 50$ eV; alternatively, the f'' component is nonzero only for $E > E_{edge} - 10$ eV (where $E_{edge} = 7{,}112$ eV).

The multilayer profile structure factor, which is the Fourier transform of the multilayer electron density profile $\rho_{ml}(z)$ can be expressed as:

$$F_{ml}(\mathbf{q}_z, E) = \sum_{j=1}^{N_j} f_j(\mathbf{q}_z, E) \exp(-2\pi i \mathbf{q}_z z_j) \propto \int_{-\infty}^{+\infty} \rho_{ml}(z) \exp(-2\pi i \mathbf{q}_z z)\, dz, \quad (2)$$

where N_j in this case includes all the atoms in the multilayer structure.

The structure factor summations can also be separated into nonresonance and resonance components as follows

$$F_{ml}(\mathbf{q}_z, E) = F_{ml}^\circ(\mathbf{q}_z) + F_{ml}'(\mathbf{q}_z, E) + iF_{ml}''(\mathbf{q}_z, E), \quad (3a)$$

where F° is the nonresonance structure factor far away from the absorption edge, F' is the resonance change in the real component of the

structure factor as a function of energy, and F'' is the resonance change in the imaginary component that is also energy dependent. As the electron density function for a finite multilayer is in general asymmetric, the resulting structure factor will have both symmetric and asymmetric components. Combining this fact with Eqs. 1, 2, and 3a above, the multilayer profile structure factor can then be expressed as:

$$F_{ml}(\mathbf{q}_z, E) = F^s_{ml}(\mathbf{q}_z) + iF^a_{ml}(\mathbf{q}_z) + \sum_{j=1}^{N_j} f'_j \exp(-2\pi i \mathbf{q}_z z_j) + i\sum_{j=1}^{N_j} f''_j \exp(-2\pi i \mathbf{q}_z z_j), \quad (3b)$$

where F^s is the nonresonance symmetric component of the structure factor, and F^a is the nonresonance antisymmetric component; the f' and the f'' resonance components of the atomic scattering factor for the jth resonant atoms positioned within the multilayer profile structure z_j are now summed only over the resonant atoms N_j.

For a five monolayer lipid film having a surface layer of highly specific, electrostatically bound cytochrome c, there should be only one position z_j for the resonant heme iron atoms thereby introducing nonzero f' and f'' terms; see Discussion. The corrected intensity function can then be written in terms which explicitly describe the resonance effect:

$$I_c(\mathbf{q}_z, E) \propto |F_{ml}(\mathbf{q}_z, E)|^2 \simeq [F^s_{ml}(\mathbf{q}_z)]^2 + [F^a_{ml}(\mathbf{q}_z)]^2 + [F^s_{ml}(\mathbf{q}_z)][f'_j \cos(2\pi \mathbf{q}_z z_j) + f''_j \sin(2\pi \mathbf{q}_z z_j)] + [F^a_{ml}(\mathbf{q}_z)][f''_j \cos(2\pi \mathbf{q}_z z_j) - f'_j \sin(2\pi \mathbf{q}_z z_j)]. \quad (4)$$

For iron atoms at the edge, $f' \simeq -8$ electrons, and $f'' \simeq -f'/2 \simeq +4$ electrons. For a structure having many more atoms that are not at resonance, the $F^s_{ml}(\mathbf{q}_z)$ and the $F^a_{ml}(\mathbf{q}_z)$ terms dominate. Thus, $|f'|^2$ and the $|f''|^2$ terms may be ignored, being much smaller than the other four terms of Eq. 4.

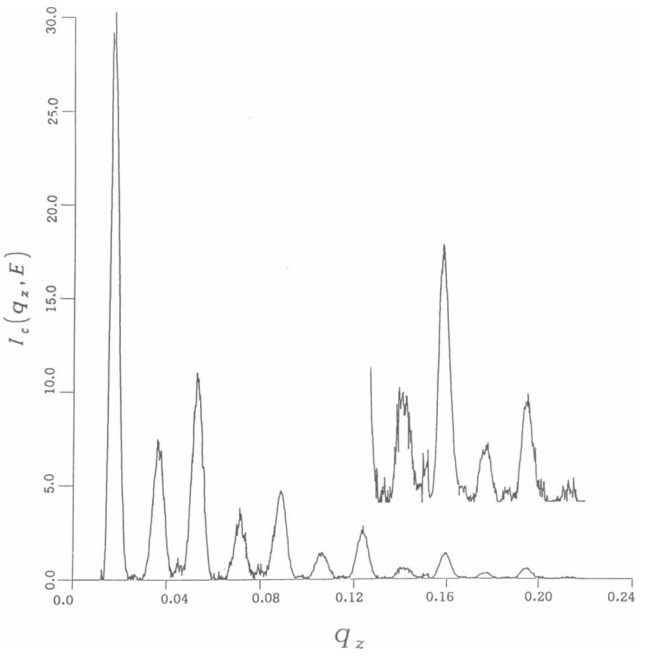

FIGURE 1 The corrected meridional intensity $I_c(\mathbf{q}_z, E_{edge})$ as a function of $\mathbf{q}_z$ (units of Å^{-1}) for an ultrathin multilayer film consisting of five monolayers of arachidic acid with an electrostatically bound surface layer of cytochrome c. The insert shows the primary diffraction orders 1 = 8–12 on an expanded scale.

RESULTS

Fig. 1 shows the corrected meridional intensity function $I_c(\mathbf{q}_z, E_{edge})$, where E_{edge} = 7,112 eV for the cytochrome c heme iron atoms, for an ultrathin lipid multilayer film consisting of five monolayers of arachidic acid with an electrostatically bound monolayer of cytochrome c. The intensity function shown in Fig. 1 extends to a greater value of $\mathbf{q}_z$ than the lamellar diffraction pattern published previously for an equivalent sample ($\mathbf{q}_z$ = 0.215 Å^{-1}, equivalent to a spatial resolution of 4.65 Å, versus $\mathbf{q}_z$ = 0.132 Å^{-1}, reference 7); however, the diffraction patterns from these two separate experiments are quantitatively similar over the first seven diffraction orders.

As before, the corrected intensity function of Fig. 1 is indicative of lamellar diffraction from asymmetric multilayer profiles of finite extent (7–10). Asymmetry is manifest primarily as nonzero minima between primary diffraction maxima. In addition, the broad resolved shape of the maxima (in $\Delta\mathbf{q}_z$) and the shifts in their positions (in $\mathbf{q}_z$) away from l/d_o (where d_o is the profile extent of the average bilayer in the multilayer, and 1 is an integer) result from the fact that the multilayer profiles are of limited extent (7–10).

The difference lamellar x-ray diffraction patterns between intensity functions measured at two energies from the five monolayer lipid/cytochrome c film were calculated and are shown in Fig. 2; $\mathbf{q}_z$ in this figure extends over the first five primary diffraction maxima (i.e., l = 1 to 5). As the F' and F'' resonance terms of Eq. 3a have significant magnitude only for $E > E_{edge} - 50$ eV (see also Eq. 1), the difference between the x-ray diffraction patterns at $E = E_{edge} - 100$ eV and $E = E_{edge} - 50$ eV should be nearly zero. As can be seen in Fig. 2 *A*, this difference x-ray diffraction pattern shows a relatively small energy dependent effect (presumably due to the "wings" of the F' term extending into this energy region). On the other hand, Fig. 2 *B* shows a difference x-ray diffraction pattern for $E = E_{edge}$ (where the F' effect is maximal, and $F'' \simeq -F'/2$) and $E = E_{edge} - 50$ eV, revealing an energy-dependent effect that is substantially greater than that of Fig. 2 *A* for the same energy difference of 50 eV. Likewise, Fig. 2 *C* shows a difference x-ray diffraction pattern for $E = E_{edge} + 100$ eV (where the F'' effect is near the maximum) and $E = E_{edge} - 100$ eV, revealing a substantial energy-dependent effect. It should be noted that the resonance effects seen in Fig. 2, *B* and *C* are not due to systematic errors, such as the scaling of the meridional intensity functions and the calibration of $\mathbf{q}_z$

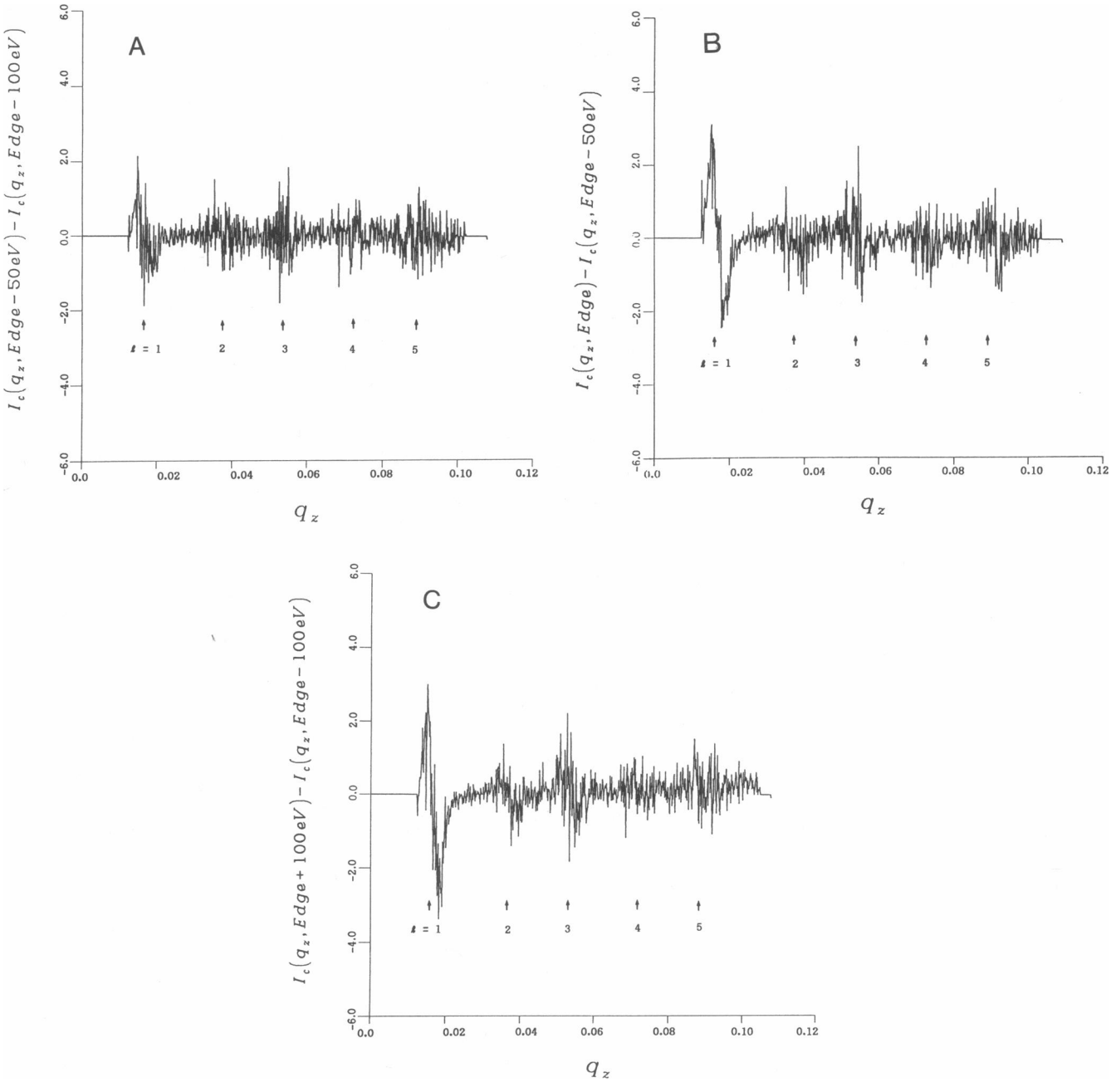

FIGURE 2 The difference intensity function between the corrected intensity functions $I_c(\mathbf{q}_z, E)$ measured at two energies for an ultrathin multilayer film consisting of five monolayers of arachidic acid with an electrostatically-bound surface layer of cytochrome *c*. (*A*) $I_c(\mathbf{q}_z, E = E_{edge} - 50\text{ eV})$ minus $I_c(\mathbf{q}_z, E = E_{edge} - 100\text{ eV})$; (*B*) $I_c(\mathbf{q}_z, E = E_{edge})$ minus $I_c(\mathbf{q}_z, E = E_{edge} - 50\text{ eV})$; (*C*) $I_c(\mathbf{q}_z, E = E_{edge} + 100\text{ eV})$ minus $I_c(\mathbf{q}_z, E = E_{edge} - 100\text{ eV})$, where $E_{edge} = 7{,}112$ eV, the resonance value for the cytochrome *c* heme Fe atom. $\mathbf{q}_z$ extends over the first five diffraction orders (1 = 1 to 5).

and $\mathbf{q}_z = 0$ with x-ray energy, or an energy-dependent lamellar background scattering function. Such possible errors have been investigated for similar finite multilayers of arachidic acid in the absence of a surface monolayer of cytochrome *c* over a much greater 1,000 eV range. In the absence of the resonant heme iron atoms, such difference x-ray diffraction patterns (analogous to those described above) were entirely featureless within the noise levels of Fig. 2.

The inherently asymmetric profile structure of the

ultrathin multilayer film used here (as evident from the corrected meridional intensity function of Fig. 1) requires that the method used to determine the multilayer relative electron density profile cannot assume centrosymmetric phases. The box refinement procedure, which utilizes the simple boundary condition that the multilayer relative electron density profile structure is zero outside of a box of length D_n (where D_n is the extent of the multilayer profile composed of n monolayers), has been effectively applied to meridional diffraction data from finite multilayer systems to produce correct multilayer profiles (7, 16, 17). This technique is an iterative procedure that begins with the application of an arbitrary phase for each point in $\mathbf{q}_z$, derived from the Fourier transform of some arbitrary trial function, to the modulus of the experimental structure factor, $[I_c(\mathbf{q}_z, E)]^{1/2}$; a trial function such as a ramp function or a phase-shifted sinusoidal function will thus initiate the iteration with noncentrosymmetric phases.

However, the multilayer electron density profiles derived from the box refinement procedure employing arbitrary trial functions are, to some extent, dependent on the trial function, and are not necessarily unique solutions. Various trial functions are therefore used to produce multilayer relative electron density profiles using the box refinement procedure; it has been previously found that the application of numerous arbitrary trial functions will lead to qualitatively similar multilayer profile structures (7–10). For the results presented here, it was found that a number of arbitrary trial functions produced multilayer relative electron density profiles generally containing the expected features of fatty acid bilayer/monolayer profiles (e.g., electron deficient terminal methyl groups and electron dense carboxyl groups separated by dimensionally appropriate intermediate density methylene chain groups) with an additional electron density feature at the multilayer surface; in addition, these profiles have the proper number of monolayers, as independently verified by the multilayer profile autocorrelation functions (see reference 7).

While the arbitrary trial functions all produced the expected electron density profile, a model five-monolayer lipid multilayer profile consisting of Gaussian functions (without an electron density contribution from cytochrome c) was calculated and used as a trial function in the refinement protocol in order to minimize the effects of

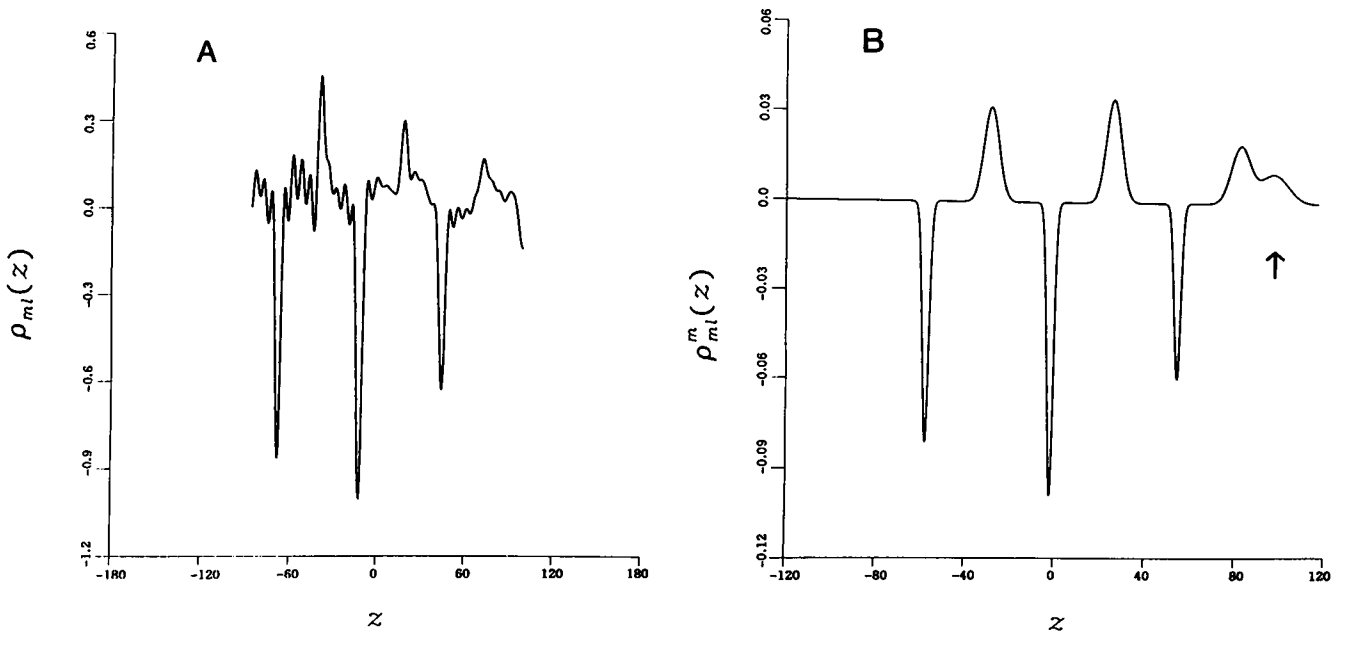

FIGURE 3 (A) The multilayer relative electron density profile $\rho_{ml}(z)$, as derived for nonperiodic multilayer lattices via the box-refinement phasing method, for the ultrathin film consisting of five monolayers of arachidic acid with a bound surface monolayer of cytochrome c. The alkylated glass substrate would appear to the left of $z \approx -60$ Å, while the carboxyl group surface of the multilayer occurs at $z \approx 60$ Å. (B) The model relative electron density profile $\rho^{m}_{ml}(z)$ for a five monolayer arachidic acid multilayer with a bound surface layer of cytochrome c, using 7 Gaussian functions. The model parameters (peak height, full width at half maxima, and peak position) were initially determined from a previously derived relative electron density profile (see reference 7), then refined as described in the text to the point where $\rho_{ml}(z)$ and $\rho^{m}_{ml}(z)$ have the same structure factors (amplitude and phases). The model electron density profile is thereby fully consistent with the derived electron density profile of Fig. 3 A; note that the methyl group to carboxyl group distances of the first, third, and fifth monolayers are greater than those of the second and fourth (8–10).

errors in the meridional intensity function (7). This five-monolayer lipid multilayer model was calculated based on the electron density profiles derived in previously reported experiments (7). Fig. 3 *A* shows the multilayer relative electron density profiles generated from this trial function after 20 iterations by applying the box refinement method to the corrected intensity function of Fig. 1. The box used in applying the boundary constraint was ±120 Å. The major features common to the profiles of our previous study (7) include well-defined terminal methyl group troughs at $z \approx -64$, -10, and 46 Å, while carboxyl group peaks appear at $z \approx -35$, 20, and 75 Å. The carboxyl group peak at $z \approx 75$ Å appears somewhat disordered (broadened), with an additional strong peak between 85 and 115 Å, which indicates the presence of a cytochrome *c* monolayer (similar to our previous results [7]).

In a rather different manner, a model five-monolayer lipid multilayer profile with a surface monolayer of cytochrome *c* was then calculated to represent the experimental electron density profile of Fig. 3 *A*; this model profile structure (Fig. 3 *B*) will be utilized below to analyze the energy-dependent effects of Fig. 2. A model five monolayer profile consisting of Gaussian functions located at the terminal methyl group troughs and the carboxyl group peaks of the multilayer relative electron density profile of Fig. 3 *A* was constructed, which also included a peak of electron density (20 Å width) overlapping the outer carboxyl group peak to represent the cytochrome *c* contribution (Fig. 3 *B*). This initial model multilayer profile structure, $\rho_m(z, E)$, was used as the trial function to calculate the multilayer profile structure $\rho_c(z, E)$ of the first and tenth iteration via the box refinement method. The parameters of the Gaussian functions of the model electron density profile of Fig. 3 *B* were then varied (magnitude, width, and position of each function) until the characteristics of the calculated multilayer profile structure ρ_c were the same for both the first and tenth iteration. Using the box refinement method in this manner, a Gaussian function model $\rho_m(z, E)$ is found that is equivalent to experimentally derived multilayer profile structure $\rho_c(z, E)$ (as the amplitude and phases of the experimentally derived structure factor $F_c[\mathbf{q}_z, E]$ are then equal to those of the model structure factor $F_m[\mathbf{q}_z, E]$). This particular utilization of the box refinement method employs the well-known fact that the rate of convergence of the box-refinement method depends strongly on the similarity between the initial trial function and a solution.

The resonance x-ray diffraction effects can then be calculated using the model electron density profile of Fig. 3 *B* and Eq. 4. The model electron density profile of Fig. 3 *B* can be separated into symmetric ($\rho^s_{ml}[z, E]$) and antisymmetric ($\rho^a_{ml}[z, E]$) components. The Fourier transform of the symmetric and antisymmetric electron density components therefore produce the symmetric and antisymmetric structure factor components ($F^s_{ml}[\mathbf{q}_z, E]$ and $F^a_{ml}[\mathbf{q}_z, E]$, respectively). Thus, the energy dependence of the intensity function $I_m(\mathbf{q}_z, E)$ can be calculated from Eq. 4, using the symmetric and antisymmetric structure factor components generated from the model electron density profile of Fig. 3 *B* and values for the $F'(\mathbf{q}_z, E)$ and $F''(\mathbf{q}_z, E)$ effects for the cytochrome *c* heme Fe atoms located in a plane at any position z_j. The magnitudes of the $F'(\mathbf{q}_z, E)$ and $F''(\mathbf{q}_z, E)$ effects are calculated by first assuming that (*a*) the cytochrome *c* is a homogeneous sphere of radius 17.4 Å, with average electron density of 0.39 $e/Å^3$, (*b*) the cytochrome *c* is located on the surface of the lipid multilayer as a hexagonally close-packed monolayer of protein (7); (*c*) the average electron densities of the lipid polar head groups, hydrocarbon chain methylene groups, and terminal methyl groups are 0.44 $e/Å^3$, 0.33 $e/Å^3$, and 0.13 $e/Å^3$, respectively; (*d*) the average electron density of water is 0.33 $e/Å^3$ (it is assumed that volume on the surface of the lipid multilayer profile structure that is not occupied by cytochrome *c* or the lipid head groups must be occupied by water); and (*e*) at the absorption edge, $f'_{Fe} \simeq -8$ electrons and $f''_{Fe} \simeq +4$ electrons. Therefore, the projected electron density at any point in the multilayer profile along *z* can be calculated by using the equation:

$$\rho_{ml}(z, E) = \rho_{lipid}(z) + \rho_{protein}(z) + \rho_{water}(z) + \rho_{Fe}(z, E). \quad (5)$$

Thus, the resonance effect on the multilayer structure factor $F_{ml}(\mathbf{q}_z, E)$ (that contains only the f' and f'' components of the Fe atoms) can be calculated accordingly:

$$\Delta F_{ml}(\mathbf{q}_z, \Delta E) \propto \int_{-\infty}^{+\infty} [\rho_{Fe}(z, E_1) - \rho_{Fe}(z, E_2)] \exp(-2\pi i \mathbf{q}_z z)\, dz. \quad (6)$$

Model meridional intensity functions $I_m(\mathbf{q}_z, E)$ were thus produced using Eq. 4 for z_j at 1 Å intervals, at $E = E_{edge}$, $E > E_{edge} + 50$ eV, and $E < E_{edge} - 50$ eV. Subsequently, calculated difference intensity functions were produced by subtracting the pairs of $I_m(\mathbf{q}_z, E_{edge}) - I_m(\mathbf{q}_z, E_{edge} - 50$ eV) (for example see Fig. 4), and $I_m(\mathbf{q}_z, E > E_{edge} + 50$ eV) $- I_m(\mathbf{q}_z, E < E_{edge} - 50$ eV) (for example see Fig. 5). Note that these model difference intensity functions can exhibit derivative-like features at positions along $\mathbf{q}_z$ that correspond to the primary diffraction maxima at $1 \simeq (1$ to $6)/d_o$. For example, the positions of the first five primary diffraction maxima of Fig. 4 *A* and 5 *A* (where the iron position is located at $z_j = 103$ Å) have positive derivative features; alternatively, some of the features of Figs. 4 *B* and 5 *B* (where $z_j = 110$ Å) show negative derivative-like characteristics (i.e., at $\mathbf{q}_z = 0.051, 0.068$, and 0.073 $Å^{-1}$ of Fig. 5 *B*, positioned at

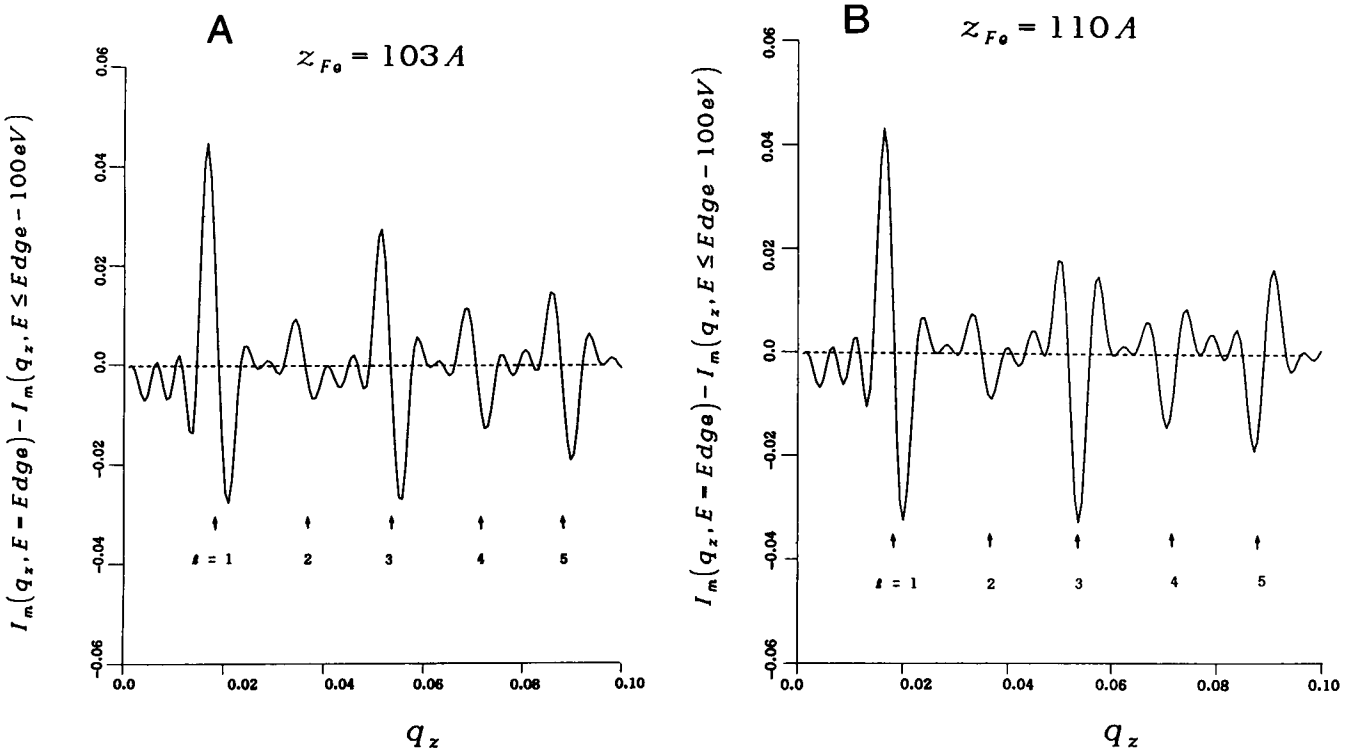

FIGURE 4. Intensity functions $I_m(\mathbf{q}_z, E)$ were calculated from the model electron density profile of Fig. 3 *B*, using Eq. 4 (see text) to include the resonance effect of one iron atom per cytochrome *c*. The position of the iron atoms along the electron density profile structure (z_j) was varied (by 1 Å steps); the difference intensity function between two calculated model intensity functions, $I_m(\mathbf{q}_z, E_1)$ and $I_m(\mathbf{q}_z, E_2)$, was calculated for each value of z_j. In this figure, E_1 = Edge and $E_2 < E_{edge} - 100$ eV. (*A*) $z_j = 103$ Å, which produces features that are virtually identical to the experimental function of Fig. 2 *B*; (*B*) $z_j = 110$ Å. Note that in *B*, the difference intensity function at the position of the fifth primary diffraction maxima has a derivative of opposite sign to *A*, and that at the positions of the third and fourth primary diffraction maxima negative peaks are observed (see text and Table 1). $\mathbf{q}_z$ extends over the first five primary diffraction maxima (1 = 1 to 5).

$1 \simeq 3/d_o$, $4/d_o$, and $5/d_o$), or simply negative or positive characteristics (i.e., at $\mathbf{q}_z = 0.051$ and 0.068 Å^{-1} of Fig. 4 *B*, positioned at $1 \simeq 3/d_o$ and $4/d_o$). For every value of z_j, two difference intensity functions were calculated: (*a*) $I_m(\mathbf{q}_z, E_{edge})$ minus $I_m(\mathbf{q}_z, E < E_{edge} - 50$ eV); and (*b*) $I_m(\mathbf{q}_z, E > E_{edge} + 50$ eV) minus $I_m(\mathbf{q}_z, E < E_{edge} - 50$ eV), and the characteristics of the difference functions at the primary diffraction maxima at $1 = 1/d_o$ to $6/d_o$ were tabulated. Tables 1, A and B show a partial listing of these calculated results for $I_m(\mathbf{q}_z, E_{edge})$ minus $I_m(\mathbf{q}_z, E < E_{edge} - 50$ eV) and $I_m(\mathbf{q}_z, E > E_{edge} + 50$ eV) minus $I_m(\mathbf{q}_z, E < E_{edge} - 50$ eV), respectively, where "$+D$" represents a positive derivative, "$-D$" a negative derivative, "+" a positive peak, and "−" a negative peak; the experimentally observed features, taken from Fig. 2, *B* and *C* respectively, are shown at the top of Tables 1, A and B. As can be seen from these tables and the Discussion section, the qualitative comparisons between these characteristics of the experimental difference intensity functions versus the model difference intensity functions are sufficient to severely restrict the locations of the heme Fe atoms within the cytochrome *c* monolayer along *z* in the multilayer profile projection. We note that we chose to make only such qualitative comparisons between the shapes of the features in the measured and calculated difference intensity functions in the neighborhood of the primary diffraction orders because of the signal to noise level in the measured functions (Fig. 2). With the availability of position-sensitive photon counting x-ray detection, it should be straightforward to improve the signal to noise ratio for the measurement of resonance diffraction effects not only within the primary diffraction orders, but also in their associated secondary diffraction maxima for these finite multilayers. Therefore, a significant increase in the accuracy of the location of resonant atom(s) within the multilayer profile projection would be expected.

DISCUSSION

In a previous study, it was shown that resonance x-ray diffraction effects from cytochrome *c* (having a heme-

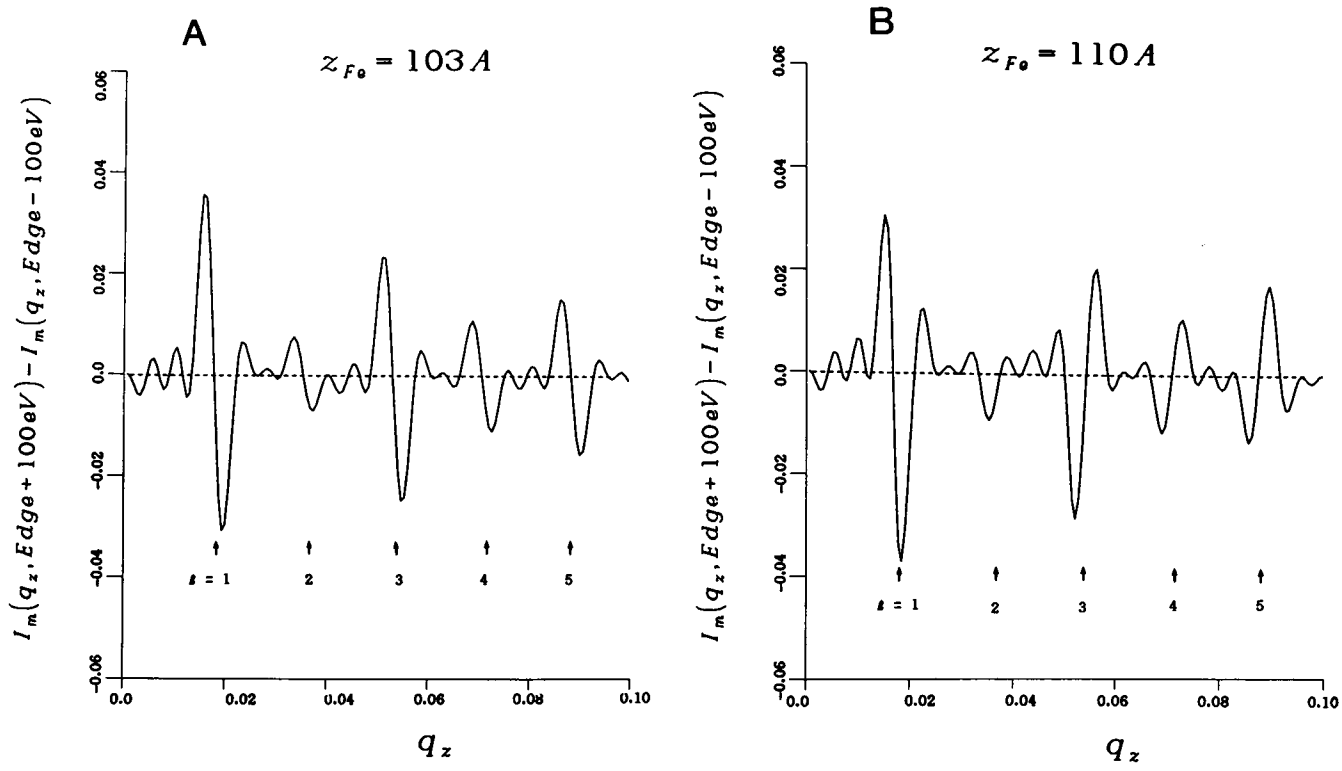

FIGURE 5 In this figure, $E_1 > E_{edge} + 100$ eV and $E_2 < E_{edge} - 100$ eV. (*A*) $z_j = 103$ Å, which produces features that are virtually identical to the experimental function of Fig. 2 *C*; (*B*) $z_j = 110$ Å. Note that in *B*, the difference intensity function at the positions of the third, fourth, and fifth primary diffraction maxima have a derivative of opposite sign to *A*, and that at the position of the second primary diffraction maxima a negative peak is observed (see text and Table 1). $\mathbf{q}_z$ extends over the first five diffraction orders (1 = 1 to 5).

associated metal atom) could be measured on the lamellar reflections from oriented, thick multilayers of a reconstituted membrane containing a photosynthetic reaction center/cytochrome *c* complex (11–13). Furthermore, a model refinement analysis of these differential resonance diffraction effects showed that the position of the heme-associated metal atom of the cytochrome *c* was restricted to a 3Å strip in the membrane electron density profile (12).

Although the procedural details of the model refinement analysis used in these previous resonance x-ray diffraction experiments (12) were different from the present model analysis, the underlying strategies are similar, and the accuracy of the results are also similar. In both cases, the structural organization of the molecular components within the multilayer profile was known independently from previous diffraction experiments; thus, a model refinement procedure was developed that varied only the position of the resonance scattering metal atoms within a model multilayer profile structure in order to reproduce the resonance effect in calculated lamellar diffraction patterns. As in our previous resonance x-ray diffraction experiments (12), the accuracy of determination of the metal atom profile positions simply depends on the accuracy of measuring the resonance x-ray diffraction effects (usually expressed as a difference between the diffraction at the resonance energy and a nonresonance energy). The number of possible positions of the resonance scattering atoms within the profile structure generally decreases dramatically with the number of primary diffraction maxima $I_c(\mathbf{q}_z \sim 1/d_o)$ for which the resonance effects are accurately measured.

It should be noted that the observed resonance diffraction effects (Fig. 2) are somewhat greater than the calculated effects (Figs. 4 and 5). Namely, the measured resonance diffraction effects for the primary diffraction order 1 = 1 and 1 = 3 shown in Fig. 2, *B* and *C* are ~10% and 7%, respectively of the amplitudes of the corresponding diffraction orders in Fig. 1. The corresponding calculated resonance diffraction effects for the orders 1 = 1 and 1 = 3 in Figs. 4 *A* and 5 *A* are ~4% and 3%, respectively. This small discrepancy between the magnitudes of the measured and calculated effects of approximately two suggests that the amplitudes of the features producing the electron density contrast in the multilayer profile $\Delta\rho_{ml}(z)$ giving rise to $F^{s,a}_{ml}(\mathbf{q}_z)$ in Eq. 4 have been

TABLE 1A Model difference intensity features: $I_m(E - \text{Edge}) - I_m(E < \text{Edge})$

Position Z_j	First order	Second order	Third order	Fourth order	Fifth order
Experimentally observed features	+D	+D	+D	?	+D
120	+D	−D	+D	+D	−D
115	+D	−	−D	+	+D
110	+D	+D	−	−	−D
107	+D	+D	+D	+D	−
105	+D	+D	+D	+D	+D
103	+D	+D	+D	+D	+D
101	+D	+D	+D	+D	+D
99	+D	+D	+D	+D	+D
98	+D	+D	+D	+D	+D
97	+D	+	+D	+	+
95	+	−D	−D	−	+D
90	−D	+D	−D	−	+
85	−D	+	−D	+	−D
80	−	+	+D	−D	+D
75	+D	−D	+D	+D	−D
70	+D	−	−D	+	+D
65	+D	−	−	−D	−D
60	+D	+D	+D	+D	+D
55	+D	+	+	+	+
50	+	+	−D	−	−
45	+	−	−	+D	+
40	−D	−	+D	+	−
35	−	−	+	−	+
30	−	+	−	+	−
25	−	+	−	+	−
20	−	−D	+	−	+
15	−	−	+	+	−
10	+D	−	−	+	+
5	+	+D	−	−	−

overestimated. Specifically, the chain terminal methyl group features dominate these arachidic acid multilayer profiles (Fig. 3, *A* and *B*) and their contrast with the chain methylene groups was estimated to be 0.2 $e/Å^3$ (0.33 $e/Å^3$ − 0.13 $e/Å^3$). A reduction of the contrast of these features to 0.07–0.1 $e/Å^3$ (a factor of ~2) produces agreement between the magnitudes of the measured and calculated resonance diffraction effects and simply requires a somewhat lesser degree of ordering of the terminal methyl groups in the multilayer profile as compared with that in single crystals.

Nevertheless, we note that the general features of the energy dependence of the measured meridional diffraction intensities $I_c(\mathbf{q}_z, E)$ were closely matched by the calculated meridional diffraction intensities $I_m(\mathbf{q}_z, E)$ for the appropriate values of z_j in the resonance diffraction analysis; most importantly, it is the form or shape of these features of the energy dependence that determines the possible positions of the resonant atoms within the profile structure (12).

The results of the previous x-ray diffraction studies of ultrathin lipid multilayer films with electrostatically bound cytochrome *c* established the position of the protein on the surface of the lipid films. Therefore, it was reasonable to expect that the location of the heme iron atom would be in the region of 85–115 Å in the multilayer profile (at the surface of the lipid film; see Fig. 3). As can be seen from the comparison of the first three diffraction maxima of Tables 1, *A* and *B*, the model refinement analysis of the resonance diffraction effects restricts the location z_j of the heme iron atom to region of 98–105 Å (Table 1A) and 98–104 Å (Table 1B), both of which are within the region of the cytochrome *c* electron density. Combining the information from both tables, the only region that satisfies the two separate measurements (the difference of $I[E = \text{Edge}] - I[E < \text{Edge} - 50\text{ eV}]$ and $I[E > \text{Edge} + 50\text{ eV}] - I[E < \text{Edge} - 50\text{ eV}]$) is 98–104 Å. Although there is greater uncertainty in the measurement of the resonance diffraction effects for the

TABLE 1B Model difference intensity features: $I_m(E > \text{Edge}) - I_m(E < \text{Edge})$

Position Z_j	First order	Second order	Third order	Fourth order	Fifth order
Experimentally observed features	+D	+D	+D	?	?
120	−	−D	+D	−	−D
115	−	−D	−D	+	+D
110	+D	−	−D	−D	−D
107	+D	+D	−	−	−D
105	+D	+D	+D	+D	−
104	+D	+D	+D	+D	+D
103	+D	+D	+D	+D	+D
101	+D	+D	+D	+D	+D
99	+D	+D	+D	+D	+D
98	+D	+D	+D	+D	+D
97	+D	+	+	+	−
95	+	−	+D	+	−D
90	−D	−	+	−D	+D
85	−D	+D	−D	+D	−D
80	−	+	+D	−D	+D
75	+D	−D	+D	+D	−D
70	+D	−	−D	+	+D
65	+D	−	−D	+	+
60	+D	−	−	−	−D
55	+D	+D	+D	+D	+D
50	+D	+	+	+	−D
45	+	+	−	−	+D
40	+	−	−	+	−D
35	+	−	+	−	−
30	−D	−	+	−	+
25	+D	+	−	+	−
20	−	+	−	+	−
15	+D	−D	−D	−	+
10	−	−	+	+	+
5	−	−	−	−	−

higher order diffraction maxima (i.e., the fourth order difference of Fig. 2 *B*, the fourth order difference of Fig. 2 *C*, and the fifth order difference of Fig. 2 *C*), the model refinement analysis of these resonance diffraction effects presented here further supports the restriction of the location of the resonant atoms to the strip 98 Å $\leq z_j \leq$ 104 Å.

In another study, optical linear dichroism was used to determine the average orientation of the cytochrome *c* molecules electrostatically bound to the surface of an ultrathin arachidic acid multilayer film; the dichroic ratio for the α-band absorption at 550 nm indicated that the heme of the electrostatically bound monolayer of cytochrome *c* lies, on average, nearly parallel to the surface of the ultrathin multilayer surface (J.M. Pachence, J. Vanderkoii, P.L. Dutton, and J.K. Blasie, manuscript submitted for publication). Based on the cytochrome *c* structure at atomic resolution (19), this optical linear dichroism result is fully consistent with the resonance diffraction experiment which locates the Fe atom near the center of the cytochrome *c* electron density profile. Given the location of the heme group within the cytochrome *c* molecule (central relative to the two minor axes, and near the edge of the major axis of the prolate ellipsoid [20]), these two results would orient the major axis of the cytochrome *c* ellipsoid parallel to the surface of the multilayer film; the previous x-ray diffraction studies on these cytochrome *c*/ultrathin lipid multilayer films showed that the projection of the cytochrome *c* monolayer onto the profile axis *z* was 20 to 25 Å (the length of the minor axes) which would also indicate that the major axis of the cytochrome *c* is parallel to the surface of the multilayer film (7).

Fig. 6 presents a schematic of the structural information that has been obtained from resonance and nonresonance x-ray diffraction for the arachidic acid multilayer films with an electrostatically bound monolayer of cytochrome *c*. The first monolayer of lipid is associated with the hydrocarbon chains of the OTS-coated glass surface, which begins at $z = -60$ Å (7–9). The odd number (1st, 3rd, etc.) monolayers contain all *trans* chain configurations oriented normal to the substrate plane. The even number monolayers contain all *trans* chain configurations and have been shown to exhibit a tilt of 33°–36° with respect to the normal to the substrate plane (18). The last lipid monolayer is significantly disordered via "kinks" and "jogs" within the hydrocarbon chain configurations, thereby somewhat disordering the surface carboxyl groups along *z* (8–10, 18). The cytochrome *c* monolayer is bound to this somewhat disordered lipid carboxyl group surface via electrostatic interactions, which restricts the cytochrome *c* translational motion to the plane of the lipid film surface (7, J.M. Pachence, J. Vanderkoii, P.L. Dutton, J.K. Blasie, manuscript submitted for publication). Finally, the vertical arrow at 101 Å depicts the position of the heme iron atom of cytochrome *c* molecules, which is shown as a dense strip within the protein molecule (as the cytochrome *c* is rotationally averaged about the *z* axis).

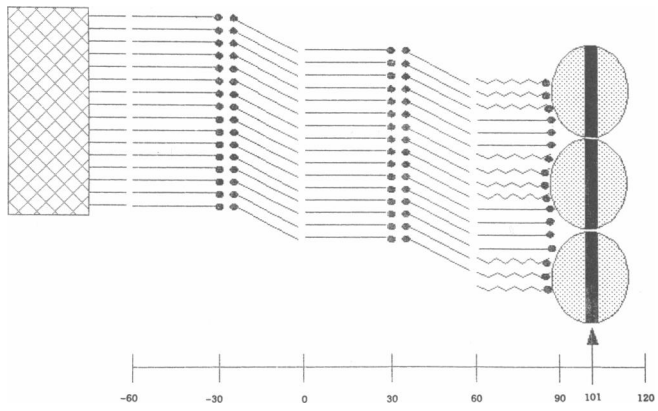

FIGURE 6 A schematic representation of the ultrathin film consisting of five monolayers of arachidic acid with a bound surface monolayer of cytochrome *c*, indicating the structural information obtained from resonance and nonresonance x-ray diffraction to date. The "rough" glass surface, denoted by the hatched lines, is coated by an OTS monolayer whose hydrocarbon chains are disordered in such a way so that the first lipid monolayer is deposited onto an apparently flat hydrophobic surface (8–10). The last monolayer whose carboxyl groups interact with cytochrome *c* is significantly disordered via "kinks" and "jogs" defects within the hydrocarbon chains. It has also been shown that the even-numbered monolayers have all *trans* hydrocarbon chain configurations which are tilted with an angle of 33°–36° with respect to the normal to the substrate surface, while the odd-numbered monolayers have all *trans* chain configurations oriented normal to the substrate surface. The vertical arrow represents the profile position along *z* of the cytochrome *c* heme Fe atoms (between 98 and 104 Å).

The resonance diffraction studies reported here clearly show the utility of these methods as applied to ultrathin, nonperiodic multilayer films. In the near future, these resonance diffraction methods will be applied to ultrathin multilayer films having a surface layer of covalently bound protein (such as cytochrome *c*), as well as complexes of membrane proteins and their ligands (such as cytochrome *c* with cytochrome oxidase).

This work was supported by National Institutes of Health grants GM 33525 and RR01633

Received for publication 5 July 1988 and in final form 30 March 1989.

REFERENCES

1. Pachence, J. M., P. L. Dutton, and J. K. Blasie. 1979. Structural studies on reconstituted reaction center-lipid membranes. *Biochim. Biophys. Acta.* 548:348–373.

2. Pachence, J. M., P. L. Dutton, J. K. Blasie. 1983. A structural investigation of cytochrome *c* binding to photosynthetic reaction centers in reconstituted membranes. *Biochim. Biophys. Acta.* 724:6–19.
3. Henderson, R., and P. N. T. Unwin. 1975. Three-dimensional model of purple membrane obtained by electron microscopy. *Nature (Lond.).* 257:28–32.
4. Deisenhofer, J., O. Epp, K. Miki, R. Huber, and H. Michel. 1984. Structure of the protein subunits in the photosynthetic reaction centre of *Rhodopseudomonas viridis* at 3 Å resolution. *Nature (Lond.).* 318:618–624.
5. Blasie, J. K., M. Erecinska, S. Samuels, and J. S. Leigh. 1978. The structure of a cytochrome oxidase-lipid model membrane. *Biochim. Biophys. Acta.* 501:33–53.
6. Pachence, J. M., P. L. Dutton, and J. K. Blasie. 1981. The reaction center profile structure derived from neutron diffraction. *Biochim. Biophys. Acta.* 635:267–283.
7. Pachence, J. M., and J. K. Blasie. 1987. The location of cytochrome *c* on the surface of ultrathin lipid multilayer films using x-ray diffraction. *Biophys. J.* 52:735–747.
8. Skita, V., M. Filipkowski, A. F. Garito, and J. K. Blasie. 1986. Profile structures of very thin multilayers by x-ray diffraction using direct and refinement methods of analysis. *Phys. Rev. B.* 34:5826–5837.
9. Skita, V., W. Richardson, M. Filipkowski, A. F. Garito, and J. K. Blasie. 1987. Overlayer-induced ordering of the disordered surface monolayer in Langmuir-Blodgett thin films. *J. Physique.* 47:1849–1855.
10. Fischetti, R., M. Filipkowski, A. Garito, and J. K. Blasie. 1987. Profile structures of ultrathin periodic and nonperiodic multilayer films containing a disubstituted diacetylene by high resolution x-ray diffraction. *Phys. Rev. B.* 37:4714–4726.
11. Stamatoff, J., P. Eisenberger, J. K. Blasie, J. M. Pachence, A. Tavormina, M. Erecinska, P. L. Dutton, and G. Brown. 1982. The location of redox centers in biological membranes determined by resonance x-ray diffraction. I. Observation of the resonance effect. *Biochim. Biophys. Acta.* 679:177–187.
12. Blasie, J. K., J. M. Pachence, A. Tavormina, M. Erecinska, P. L. Dutton, J. Stamatoff, P. Eisenberger, and G. Brown. 1982. The location of redox centers in biological membranes determined by resonance x-ray diffraction. II. Analysis of the resonance diffraction data. *Biochim. Biophys. Acta.* 679:188–197.
13. Blasie, J. K., J. M. Pachence, A. Tavormina, P. L. Dutton, J. Stamatoff, P. Eisenberger, and G. Brown. 1983. The location of redox centers in the profile structure of a reconstituted membrane containing a photosynthetic reaction center-cytochrome *c* complex by resonance x-ray diffraction. *Biochim. Biophys. Acta.* 723:350–357.
14. Blasie, J. K., and J. Stamatoff. 1981. Resonance x-ray scattering: its use in determining spatial relationships among metal atoms within macromolecules in a non-crystalline state. *Annu. Rev. Biophys. Bioeng.* 10:451–458.
15. Sagiv, J. 1980. Organized monolayers by adsorption. I. Formation and structure of oleophobic mixed monolayers on solid surfaces. *J. Am. Chem. Soc.* 102:92–98.
16. Stroud, R. M., and D. A. Agard. 1979. Structure determination of asymmetric membrane profiles using an iterative Fourier method. *Biophys. J.* 25:495–514.
17. Makowski, L. 1981. The use of continuous diffraction data as a phase constraint. I. One-dimensional theory. *J. Appl. Cryst.* 14:734–742.
18. Fischetti, R., V. Skita, A. F. Garito, and J. K. Blasie. 1988. Asymmetry in the interior arachidic acid bilayers within ultrathin multilayers fabricated via the Langmuir-Blodgett technique. *Phys. Rev. B.* 37:4788–4791.
19. Dickerson, R. E., and R. Timkovitch. 1975. *In* The Enzymes. P. D. Boyer, editor. Vol. 11. 397–547, Academic Press Inc., New York. 397–547.